The pair correlation function of krypton in the critical region: theory and experiment

1997 J. Phys.: Condens. Matter 9 8849

(http://iopscience.iop.org/0953-8984/9/42/003)

J. Phys.: Condens. Matter **9** (1997) 8849–8871. Printed in the UK PII: S0953-8984(97)83222-5

The pair correlation function of krypton in the critical region: theory and experiment

F Barocchi†‡, P Chieux‡, R Fontana§‡, R Magli‖‡, A Meroni¶, A Parola+‡, L Reatto¶‡ and M Tau*‡

† Dipartimento di Fisica, Universitá di Firenze, Largo E Fermi 2, Firenze, Italy
‡ Institut Laue-Langevin, 156X, 38042, Grenoble Cédex, France
§ Dipartimento di Elettronica, Universitá di Firenze, Via di S Marta 3, Firenze, Italy
‖ Dipartimento di Energetica S Stecco, Universitá di Firenze, Via di S Marta 3, Firenze, Italy
¶ Dipartimento di Fisica, Universitá di Milano, Via Celoria 16, Milano, Italy
+ Istituto di Scienze Fisiche, Universitá di Milano, Via Lucini 3, Como, Italy
* Dipartimento di Fisica, Università di Parma, 43100, Parma, Italy
‡ Istituto Nazionale per la Fisica della Materia, Italy

Received 8 April 1997, in final form 3 July 1997

Abstract. We present the results of high-precision measurements of the structure factor $S(k)$ of krypton in the near-critical region of the liquid–vapour phase transition for values of k ranging from 1.5 up to 50 nm^{-1}. The experimental results are compared with a theoretical calculation based on the hierarchical reference theory (HRT) with an accurate potential which includes two- and three-body contributions. The theory is based on a new implementation of HRT in which we avoid the use of hard spheres as a reference system. With this soft-core formulation we find a generally good agreement with experiments both at large k, where $S(k)$ probes the short-range correlations, as well as at small k, where critical fluctuations become dominant. Also, for the density derivative of the pair correlation function there is an overall good agreement between theory and experiment.

1. Introduction

The static structure factor $S(k)$ is the fundamental quantity characterizing correlations between pairs of particles in a fluid. In recent years some high-precision neutron scattering measurements of $S(k)$ have been performed on several systems, particularly rare gases (see for example reference [1]). These results, with a precision of the order of a few parts per thousand, have been used both to assess the merit of different integral equations, when a given accurate potential is used and the validity of a given interaction model. The outcome of these studies is that the structure at short distance of a system like liquid krypton in various thermodynamical states can be accurately reproduced by some refined integral equations when the system is modelled by accurate interatomic potentials. These potentials must include a two-body contribution mainly determined by the low-density properties of the system as well as a three-body contribution. The three-body potential has only a small effect on short-range correlations, but its presence is essential in order to get the correct thermodynamic properties. In contrast, simplified models of the potential like the Lennard-Jones one cannot properly describe the short-range correlations in real fluids.

Of special interest is the pair correlation function of a fluid in the region of the critical point of the liquid–vapour phase transition. Here the radial distribution function $g(r)$,

0953-8984/97/428849+23$19.50

related to $S(k)$ by Fourier transformation, develops a long-range tail on top of the short-range structure which characterizes the local ordering of the fluid. This tail is a manifestation of critical fluctuations on larger and larger length scales as the critical point is approached. This is well known both experimentally and theoretically. However, no high-precision measurement of $S(k)$ in the critical region over an extended k-range has been performed. The extended k-range is essential in order to describe the two aspects of the correlations, the short-range as well as the long-range part. This is the motivation for the present measurements.

On the theoretical side, fluids in the critical region present special problems. The method of integral equation for $g(r)$ gives an appropriate treatment of correlations at short range but has difficulties in reproducing the long-range part, and all known integral equations have pathologies of some sort in the critical region. For example, the well known modified hypernetted chain [2] (MHNC) equation does not have a proper critical point with diverging correlation length ξ and isothermal compressibility κ_T [3]. The growth of long-range correlations is understood and correctly accounted for by the renormalization group (RG) approach. This scheme can be used to derive the long-wavelength behaviour of the fluid in the critical region starting from the phenomenological description of the system by an effective Hamiltonian which governs long-range density fluctuations: the so-called ϕ^4-model. The relationship between the parameters of the effective Hamiltonian and the microscopic model is not known, so the RG approach can give accurate predictions only for the universal quantities, like the critical exponents and scaling laws. Non-universal properties, like the critical temperature, the corrections to the asymptotic critical behaviour, or the short-range part of the correlation functions, are not easily handled by usual RG treatments.

The theoretical situation has changed since the introduction of the hierarchical reference theory (HRT) of fluids. This approach has been reviewed recently [4]. This is a genuine liquid-state theory in the sense that models of fluids with realistic interatomic potentials are treated. In HRT the gradual turning on of fluctuations of increasing length scale is not achieved by partial integration over fluctuations of shorter wavelength, as is customary in RG approaches. Instead, a sequence of partially coupled systems is introduced. They are defined by suitable interactions such that fluctuations with wavevector k below a cut-off Q are suppressed. As Q is moved down to zero, one recovers the fully interacting system. Asymptotically close to the critical point, HRT has the structure of the RG approach, so critical exponents, scaling laws and homogeneity arise naturally in this approach. However, HRT, unlike the RG approach, is able to give also the non-universal-part contribution to the thermodynamic properties and the short-range part of the pair correlation.

Although HRT correctly reproduces the exact critical exponents at first order in the ϵ-expansion, the numerical values at the physical dimensionality $d = 3$ (corresponding to $\epsilon = 4 - d = 1$) are about 10% away from the exact ones. However, as discussed in reference [4], the non-universal properties, like the critical temperature or critical amplitudes, are well reproduced by HRT which provides a fairly accurate description of the critical behaviour for reduced temperatures higher than $\sim 10^{-3}$. Very close to the critical point, the discrepancy between the exact values of the critical exponents and their HRT estimates becomes important, leading to appreciable deviations in the physical quantities.

HRT has been already applied to the Lennard-Jones fluids and to a model with two- and three-body interaction. The results of the present measurements of $S(k)$ for krypton allow a detailed comparison between theory and experiment to be made. As the interatomic interaction we consider the model of two- and three-body contributions which successfully described the structure factor of krypton in the dense regime. HRT is a formally exact

scheme but actual calculations require the introduction of a closure of the infinite set of equations. We truncate the set of equations at the first equation which gives the evolution of the free energy as function of Q, by means of an *ansatz* on the pair correlation function of the partially coupled system. As a reference system we do not use hard spheres as in previous applications but the actual repulsive forces of the model potential. The reason for the change of the reference system is that hard spheres represent well the effect of steep repulsive forces at high density and low temperature but this representation is less accurate at low and intermediate densities where the critical point is located. In this work we implement a closure which has been suggested recently as a way to handle smooth repulsive forces and which is inspired by what is known as the soft mean-spherical approximation (SMSA) [5].

The plan of the paper is as follows. In section 2 we discuss the experimental techniques and in section 3 we present the theoretical scheme. In section 4 we detail the interaction model and some aspects of the computations. In section 5 we present the comparison of the experimental results with the theoretical calculations, both in the region of the first maximum of the structure factor and for small values of k, of the order of 2–2.5 nm^{-1}. The final section contains some concluding remarks.

2. Experiment

The experiment was performed on the D20 diffractometer at the Institut Laue–Langevin in Grenoble. The instrument was in its standard configuration, with the 126-cell position-sensitive detector covering an angular range of 12.6° at 1445 mm from the sample position. The efficiency of each cell was calibrated to an accuracy better than 0.1%. In order to reduce parasitic air scattering, an evacuated nose was put along the scattered neutron beam path between the sample and the detector. The selected incident neutron beam wavelength was $\lambda = 0.240\,80 \pm 0.000\,01$ nm, as verified by means of Si powder diffraction. This allowed the exchanged wavevector range $1.9 < k < 50.5$ nm^{-1} to be investigated.

In order to achieve a high data collection rate and statistical accuracy, a large vanadium sample cell (56 mm height, 20.5 mm outer diameter, 0.5 mm wall thickness) was chosen. This cell was made by electron beam welding a vanadium sheet to the top and bottom using stainless steel. A hole of diameter 2 mm to accommodate the thermal sensor was drilled in each of the two stainless steel pieces.

The sample was inserted into a cryostat. In order to minimize parasitic scattering from the sample environment the cryostat was equipped with a vanadium tail (25 mm outer and 24 mm inner diameter) and an aluminium body of diameter 500 mm. The temperature recorded at the sample was stable within 0.04 K for the duration of the whole experiment. An aluminium foil of thickness 0.1 cm was wrapped twice around the sample container in order to increase its thermal conductivity. The resulting temperature gradient along the sample was estimated to be 0.02 degrees per centimetre and, to a first approximation, did not depend on the presence of the sample.

The gas handling system consisted of a line for the introduction of the fluid samples Kr and ^{3}He into the container. The line was also connected to a vacuum pump necessary for the evacuation of the circuit; a thermal compressor was used in order to achieve the high densities of the Kr samples. The pressure was measured by a pressure transducer and it was known within 0.01 bar.

The connection of the container to the fluid injection line was made via a stainless steel tubing of external diameter 0.16 cm soldered on the top of the container and exiting the cryostat through the top flange of the sample stick. A heating wire wrapped around

the injection line allowed us to maintain the part of this tubing inside the cryostat at a temperature 20 K higher than the sample one throughout, as verified by placing several thermocouples along it. In this manner, cold spots favouring sample condensation and consequent variation of the sample density in the container were avoided. The control of the temperature of the injection line and of the temperature gradient along the tubing down to the sample container was necessary to monitor the sample's thermodynamic stability.

Table 1. Densities and temperatures of the nine states investigated. The estimated uncertainty in the temperature values is 0.04 K (see the text). We also report the reduced temperature and density.

Experiment number	T (K)	ρ (nm^{-3})	$(T - T_c)/T_c$	$(\rho - \rho_c)/\rho_c)$
1	227.64	5.38 ± 0.01	0.088	−0.17
2	227.50	7.25 ± 0.01	0.087	0.11
3	217.93	7.25 ± 0.01	0.041	0.11
4	211.60	7.25 ± 0.01	0.010	0.11
5	210.32	7.25 ± 0.01	0.005	0.11
6	211.48	9.35 ± 0.02	0.010	0.43
7	218.18	9.35 ± 0.02	0.042	0.43
8	218.10	5.80 ± 0.01	0.042	−0.11
9	211.58	5.80 ± 0.01	0.011	−0.11

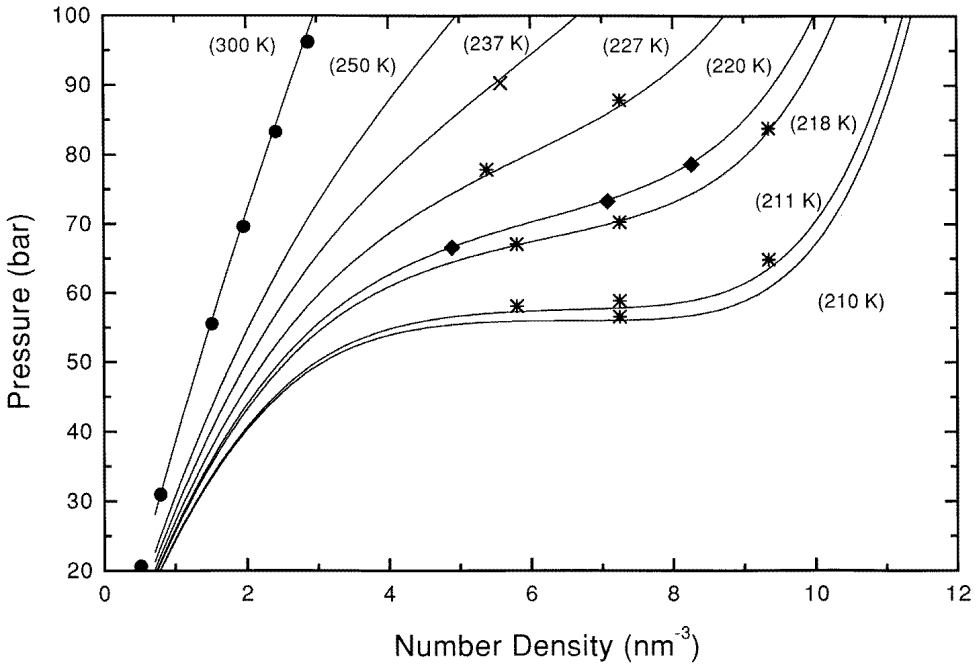

Figure 1. Krypton isotherms in the pressure–density plane from the data of reference [6]. Points marked with stars represent the states investigated in the present work, while diamonds, full circles and crosses refer to the data of references [16, 18, 19] respectively.

Nine thermodynamic supercritical states have been investigated along four different isotherms. Figure 1 shows the experimental points in the $P-V$ plane together with the states corresponding to similar previous measurements reported in the literature. The density values have been obtained from the recorded pressure and temperature measurement using the experimental thermodynamic results of Streett and Staveley [6]; the temperatures and densities of the states investigated along with the corresponding experimental uncertainties are summarized in table 1.

2.1. Data analysis

The procedure for extracting the structure factor $S(k)$ from the neutron scattering data is well established [7]. A sequence of corrections has to be applied to the measured intensities: we need to remove the scattering from the sample environment, correct for resolution, attenuation, multiple scattering and inelasticity effects, subtract the incoherent scattering contribution and normalize the data. Some of these corrections require the numerical evaluation of smoothly angle-dependent parameters which are related to:

(1) the instrument itself (wavelength, zero angular offset, instrumental resolution);

(2) the sample and its environment(sample composition, density, container geometry and dimensions); and

(3) the neutron scattering characteristics (coherent, incoherent and absorption cross sections).

The present experiment was aiming for high final accuracy (the 1% range); therefore we will detail the various steps of the data analysis and their relative importance as regards the final accuracy.

2.1.1. Angular scale definition. The first step in the data analysis was the definition of the angular scale. In fact, the nominal values of the scattering angle have to be corrected for the angular offset and because of what in the literature is known as the 'umbrella' effect [8].

The angular offset value has been determined by using the results of powder measurements, and it turned out to be 0.4865 ± 0.0018. The 'umbrella' effect occurs because each point of the sample scatters in a cone, and the scattering cones are intersected by the rectangular cells of the detectors. The finite sizes of the sample, detector and sample–detector distance modify, especially at low angles, the angular scale definition with respect to the nominal one. This problem can be treated analytically or numerically; it involves knowledge of the geometrical and instrumental parameters, like the sizes of both the sample and the detector cell, the sample–detector distance, the beam divergence, and the focusing of the monochromator. In our case the correction to the nominal angle was performed numerically using a procedure devised in [9]: it turned out to be positive and decreased on going from low to high scattering angles. Finally the Θ scale so obtained was changed into a k-scale by using Bragg's law.

2.1.2. Background and container scattering. The relatively large size of the sample container used in the experiment led to several effects. First, since the evacuated nose, placed between the sample and the detector, was adjusted for a sample diameter of 2.0 cm, the detector cells placed at both of the extremes of the multidetector had only a partial view of the container and *a fortiori* of the cryostat tail. This created a typical periodic dip in the intensity pattern at the step chosen for the multidetector displacement (see figure 2). Secondly, since a precision in the 1% range on the final $S(k)$ was required, the corrections

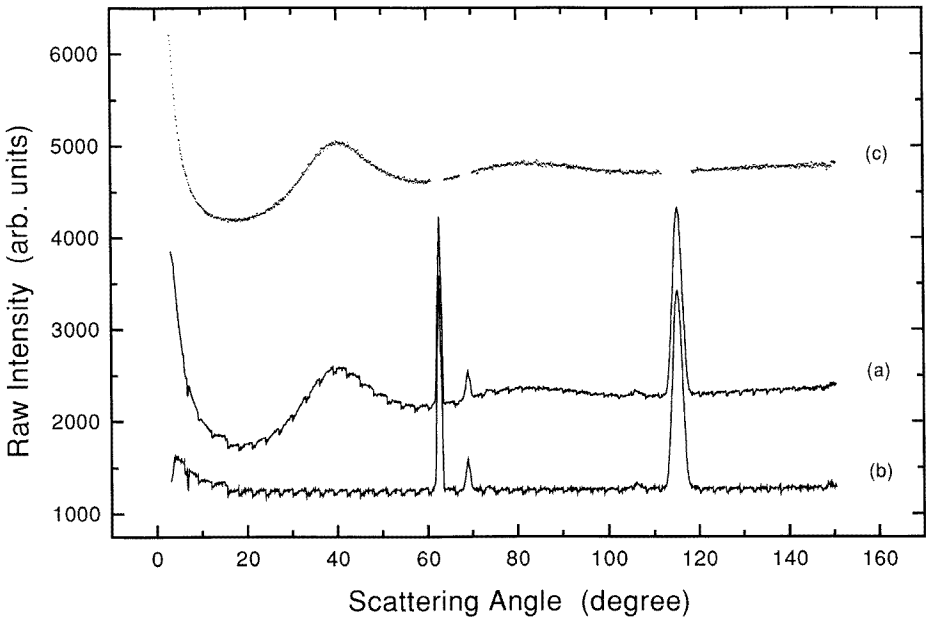

Figure 2. Curves (a) and (b) represent raw data from experiment No 3 (see table 1) and the corresponding ^{3}He intensity pattern. Curve (c) is the difference between the other two curves; this difference has been shifted upwards for clarity.

for the scattering from the container and for the sample self-attenuation are of crucial importance. This is particularly true for Kr which has a high neutron absorption cross section.

These considerations led us to the choice of the ^{3}He technique [10] for these corrections. The ^{3}He technique offers the possibility of an accurate correction for any structural detail of the container plus cryostat and background pattern. Here we briefly describe the principle of the method. The total intensity $I_T^{S,C}$ scattered by the container filled with the sample and immersed in the cryostat tail can be described as the sum of the intensity I_S scattered by the sample plus the intensity I_C^S scattered by container and cryostat, plus the intensity I_B^S coming from the background in the presence of the sample:

$$I_T^{S,C}(k) = I_S(k) + I_C^S(k) + I_B^S(k). \tag{1}$$

The scattering from the container and the environment can be directly measured. In fact, if the container is filled with an almost pure neutron absorber, like ^{3}He, and immersed in the cryostat tail, the corresponding intensity can be analogously written as

$$I_T^C(k) = I_C^{\mathrm{He}}(k) + I_B^{\mathrm{He}}(k) \tag{2}$$

where the symbols are defined in a similar way to in equation (1). The term corresponding to the intensity scattered by ^{3}He has been omitted because of the extremely low neutron scattering cross section of ^{3}He compared to its absorption cross section. When the ^{3}He density is chosen in order to match the sample transmission, $I_T^C(k)$ can be considered a direct measurement of the last two terms on the right-hand side of equation (1).

After the subtraction of I_T^C from $I_T^{S,C}(k)$ we are left with the intensity $I_S(k)$ scattered by the sample; it is still affected by effects due to multiple-scattering events and neutron

beam attenuation which will be discussed in the next section. In figure 2 the raw data corresponding to experiment No 3 of table 1, the corresponding ^{3}He intensity pattern, and the intensity $I_S(k)$ after the container and background correction are reported. The sharp peaks visible in the two lower curves are Bragg peaks due to the scattering from aluminium and vanadium present along the neutron paths in the cryostat and in the sample container. Due to their large intensity, the background subtraction described above is not able to fully correct for their presence. Therefore a blank has been left at the corresponding position in the final data.

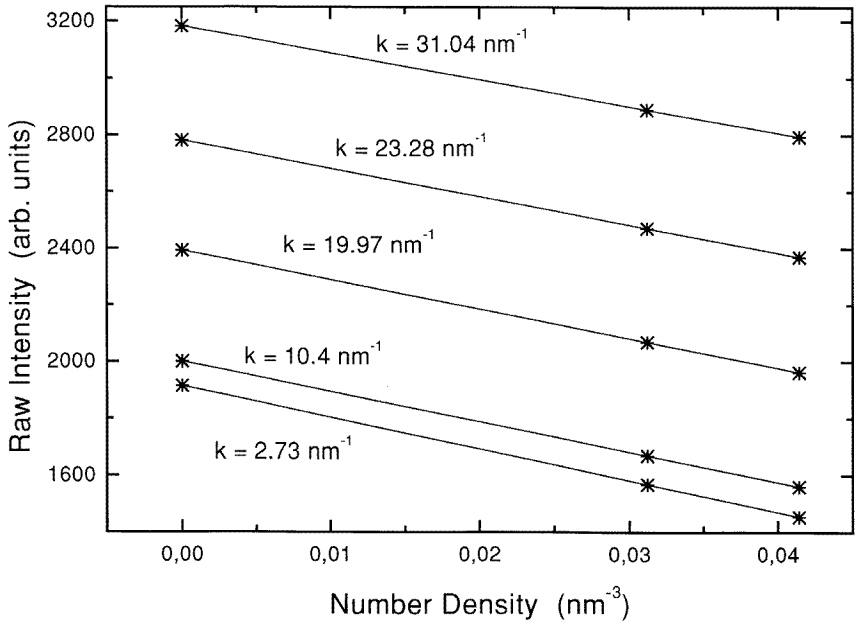

Figure 3. ^{3}He raw intensities as functions of the density for selected k-values. For the sake of clarity all of the curves except the lowest one have been shifted upwards by a constant amount. The $n = 0$ values refer to the empty-cell measurement.

We must note here that in order to save beam time we have chosen to make only three measurements with ^{3}He and one measurement with an empty container. Two of the three ^{3}He runs were at the same density but different temperatures, while the third run was at the same temperature as one of the other two but for a different density. We derived the intensities I_T^C for the other states by taking advantage of the temperature independence shown by the measured ^{3}He intensity patterns and of the linear behaviour as a function of the density exhibited for each k-value, as shown in figure 3 for selected k-values.

We estimate that the systematic error of the procedure adopted for the background correction is well within the statistical accuracy of the I_T^C-measurements which is less than eight parts per thousand.

2.1.3. Multiple scattering and attenuation. The neutrons which contribute to the intensity $I_S(k)$ scattered by the sample can be divided into those coming from a single-scattering event, $I_1(k)$, and those multiply scattered, $I_m(k)$:

$$I_S(k) = A_1(k)I_1(k) + I_m(k) \tag{3}$$

where $A_1(k)$ is the attenuation coefficient for the single scattering which will be discussed later and $I_m(k)$ also includes the attenuation of multiply scattered neutrons.

When the sample is contained in a can and this in a cryostat, like in the present case, there are two kind of process which contribute to $I_m(k)$. The first is the sequence (two or more) of scattering events which are all within the sample: we will call the resulting intensity $I_m^S(k)$. The other process is the sequence (two or more) of scattering events within the sample, the container and the cryostat tail with at least one (but not all) of them within the sample; we call the resulting intensity $I_m^E(k)$, so

$$I_m(k) = I_m^S(k) + I_m^E(k). \tag{4}$$

We must note here that multiple-scattering events all within the container and/or the cryostat tail are no longer contributing, because the corresponding intensity is included in $I_T^C(k)$ and therefore removed when this is subtracted from $I_T^{S,C}(k)$.

The evaluation of the multiple-scattering contributions can be performed numerically; in our case the sample and its environment have a cylindrical symmetry, and the multiannuli treatment of the CYLMUL code [11] is adequate. The multiple scattering could therefore be computed for each experimental situation, e.g. the Kr sample within the container and the cryostat or ^{3}He within the container and the cryostat. A few comments are necessary here. CYLMUL allows one to compute multiple scatterings within several annuli of different sizes and cross sections, each scattering event being considered as fully isotropic. The assumption of isotropy of the scattering is certainly justified for vanadium, an almost incoherent scatterer of heavy mass. However, it has been verified with a simple model [12] that after the second scattering event the memory of the initial structure factor is effectively lost also for Kr, and the twice-scattered intensity can be therefore considered as isotropic to better than 1%.

Although multiple scattering does not introduce any relevant modification of the structure, it is nevertheless the largest correction that we apply to the data, since it corresponds to about 10–15% of the corrected Kr intensity level. We estimate that systematic errors in this correction correspond to a rather flat level contribution up to $\sim$1.5% in the final Kr differential scattering cross sections. They could arise partially from uncertainties in the parameters defining the beam and the sample environment and partially from the limits of the algorithm itself such as the hypotheses made for the higher-order multiple-scattering terms.

The coefficient $A_1(k)$ in equation (3) takes into account the attenuation of both the incident and the scattered neutron beams due to the various materials of the sample environment and container as well as the sample itself. It corresponds to the coefficient $A_{S,SC}$ in the Paalman and Pings notation [13]. This parameter can be computed numerically for the once-scattered neutron; the computation requires the knowledge of the geometrical sizes and the total cross sections of the sample, container and cryostat tail. The effect of the cryostat tail is to introduce an angular dependence (less than one part per thousand) which in the present case has been neglected.

The k-dependence of the attenuation coefficient, normalized to the value taken at $k = 0$, can be well represented in a simple polynomial form of the type

$$A(k) = a + bk^2 + ck^4 \tag{5}$$

In table 2 the values of the coefficients a, b, c for the nine states investigated are reported.

2.1.4. Inelastic effects and structure factors. After the multiple-scattering contribution has been subtracted and the attenuation taken into account, the resulting intensity can be

Table 2. Values of the coefficients of the analytical representation of the self-attenuation factor $A_1(k)$ (see equation (5)).

Experiment number	a	b (10^{-5} nm^2)	c (10^{-10} nm^4)
1	1.000	0.796	2.115
2, 3, 4, 5	1.000	1.405	4.670
6, 7	1.000	2.327	8.247
8, 9	1.000	0.918	2.590

Table 3. Values of the coefficients of the analytical representation of the inelastic correction $P(k)$ (see equation (7)).

Experiment number	p_0	p_1 (10^{-5} nm^2)	p_2 (10^{-10} nm^4)
1, 2	1.008	−2.093	5.312
8, 3, 7	1.008	−2.070	5.026
9, 4, 6	1.008	−2.054	4.824
5	1.008	−2.051	4.777

expressed in term of the static structure factor $S(k)$:

$$I_1(k) = \frac{CN\sigma_s}{4\pi}\left\{\frac{\sigma_c}{\sigma_s}[S(k)-1]+1+P(k)\right\} \tag{6}$$

where: C is an instrumental constant defined as the product of the incident neutron flux times the detector efficiency and the detection solid angle; N is the number of sample atoms in the neutron beam; σ_c and σ_s are the coherent and total scattering cross sections of the sample, respectively; and $P(k)$ is the correction for inelastic processes.

The inelastic correction $P(k)$ has been evaluated in two different ways which have given the same results within a few parts per thousand. First the procedure proposed in references [14, 15] was used and secondly the perfect-gas expression for the dynamic structure factor $S(k,\omega)$ multiplied by the detector efficiency was integrated over ω [16]. The results for $P(k)$ could be well represented by using a polynomial form of the type

$$P(k) = p_0 + p_1k^2 + p_2k^4. \tag{7}$$

The values of the coefficients p_0, p_1 and p_2 for the four temperatures of the experiment are reported in table 3.

The normalization constant $C^* = CN\sigma_s/4\pi$ can be obtained by imposing the requirement that $\lim_{k\to\infty} S(k) = 1$. Since in the experimental k-range the intensity patterns exhibit marked oscillations even in the high-k region, we have fitted to the data the Verlet model [17]:

$$I(k) = \alpha\frac{\exp(-\beta k)}{k}\sin(\gamma k+\delta). \tag{8}$$

We estimate that the uncertainty in determining the normalization factor with this procedure varies from 1.7% at the lower densities (experiments 1, 8 and 9) to 0.7% for the other states.

The final structure factors have now been obtained from (6) using the value $\sigma_c/\sigma_s = 0.936$ already used in a previous study [1]. As noted in [1], a stringent test of the accuracy of the $S(k)$ so obtained is given by the condition that the Fourier transform of $(S(k)-1)/\rho$—that is, $h(r)$—equals -1 at short distances because of the essentially impenetrable core. The

presence of the experimental errors and the need for extending the data to small and large k prevent the exact fulfilment of this condition and introduce an oscillatory behaviour of $h(r)$, especially visible for small r-values. Nevertheless, we have verified that with the chosen value for σ_c/σ_s the amplitude of these oscillations is small and their shape is symmetrical about -1. As a result of the counting statistics and the data analysis procedure adopted, we estimate that the final accuracy of the structure factors obtained is within two parts per hundred.

3. Theory

We consider a system of particles interacting via two- and three-body potentials:

$$V(\boldsymbol{r}_1, \boldsymbol{r}_2, \ldots, \boldsymbol{r}_N) = \sum_{i<j}^{N} v_2(|\boldsymbol{r}_i - \boldsymbol{r}_j|) + \sum_{i<j<k}^{N} v_3(\boldsymbol{r}_i, \boldsymbol{r}_j, \boldsymbol{r}_k) \tag{9}$$

and we divide the total potential into two contributions, the first, V_R, which includes the three-body part (assumed here to be mainly repulsive) and the repulsive part of the two-body potential v_R ($v_2(\boldsymbol{r}) = v_R(\boldsymbol{r}) + w(\boldsymbol{r})$):

$$V_R(\boldsymbol{r}_1, \boldsymbol{r}_2, \ldots, \boldsymbol{r}_N) = \sum_{i<j}^{N} v_R(|\boldsymbol{r}_i - \boldsymbol{r}_j|) + \sum_{i<j<k}^{N} v_3(\boldsymbol{r}_i, \boldsymbol{r}_j, \boldsymbol{r}_k) \tag{10}$$

and the second including the attractive part w (which we assume sufficiently regular to have a Fourier transform) of the latter:

$$W(\boldsymbol{r}_1, \boldsymbol{r}_2, \ldots, \boldsymbol{r}_N) = \sum_{i<j}^{N} w(|\boldsymbol{r}_i - \boldsymbol{r}_j|) \tag{11}$$

$$V(\boldsymbol{r}_1, \boldsymbol{r}_2, \ldots, \boldsymbol{r}_N) = V_R(\boldsymbol{r}_1, \boldsymbol{r}_2, \ldots, \boldsymbol{r}_N) + W(\boldsymbol{r}_1, \boldsymbol{r}_2, \ldots, \boldsymbol{r}_N). \tag{12}$$

The thermodynamics and the structural properties of the system are evaluated via the hierarchical reference theory [20] introducing the family of partially interacting systems (Q-systems) defined by the potential

$$V_Q(\{r\}) = V_R(\{r\}) + W_Q(\{r\}) \tag{13}$$

where $\{r\}$ indicates the ensemble of coordinates $(\boldsymbol{r}_1, \boldsymbol{r}_2, \ldots, \boldsymbol{r}_N)$ and

$$W_Q(\{r\}) = \sum_{i<j=1}^{N} w_Q(|\boldsymbol{r}_i - \boldsymbol{r}_j|). \tag{14}$$

Here $w_Q(r)$ is defined by the equation

$$\tilde{w}_Q(k) = \begin{cases} 0 & \text{if } k < Q \\ \tilde{w}(k) & \text{if } k > Q \end{cases} \tag{15}$$

the tilde denoting Fourier transformation. The introduction of these Q-systems which interpolate between the model characterized only by the repulsive potential and the fully interacting system can be justified on the basis of the renormalization group theory as detailed in [20]. In the same paper the equation governing the evolution of the Helmholtz free energy as Q changes was deduced. It reads

$$-\frac{\mathrm{d}}{\mathrm{d}Q}\left(\frac{-\beta\mathcal{A}_Q}{V}\right) = \frac{Q^2}{4\pi^2}\ln\left[1 - \frac{\tilde{\phi}(Q)}{\tilde{C}_Q(Q)}\right] \tag{16}$$

where $\tilde{\phi}(k) = -\beta\tilde{w}(k)$, $\beta = 1/k_BT$, and $\mathcal{A}_Q$ and $\tilde{\mathcal{C}}_Q(k)$, the *modified* Helmholtz free energy and direct correlation function, are related to the Helmholtz free energy A_Q and direct correlation functions $\tilde{c}_Q(k)$ of the Q-system by the equations

$$\frac{-\beta\mathcal{A}_Q}{V} = \frac{-\beta A_Q}{V} - \frac{1}{2}\rho[\phi(0) - \phi_Q(0)] + \frac{\rho^2}{2}[\tilde{\phi}(0) - \tilde{\phi}_Q(0)] \tag{17}$$

$$\tilde{\mathcal{C}}_Q(k) = \tilde{c}_Q(k) + \tilde{\phi}(k) - \tilde{\phi}_Q(k) \tag{18}$$

where ρ is the density of the system. The previous equations are exact, but in order to give rise to a practical scheme they require a closure relation expressing the modified direct correlation function in terms of the free energy. In [21] a closure relation was studied extensively in the case of a Lennard-Jones system, corresponding to the position

$$\tilde{\mathcal{C}}_Q(k) = \tilde{c}_R(k) + \lambda_Q\tilde{\phi}(k) + \tilde{\mathcal{G}}_Q(k) \tag{19}$$

where $\tilde{c}_R(k)$ is the direct correlation function of the system interacting with the potential V_R, the *reference system*, whose properties are assumed to be known. In the previous studies, $\tilde{\mathcal{G}}_Q(k)$ and λ_Q were determined by the requirements

$$\tilde{\mathcal{C}}_Q(k = 0, \rho, T) = \frac{\partial^2}{\partial\rho^2}\left(\frac{-\beta\mathcal{A}_Q(\rho, T)}{V}\right) \tag{20}$$

$$g_Q(r) = 0 \qquad \text{if } r < d \tag{21}$$

corresponding respectively to the compressibility sum rule and the core condition on a diameter d. This approximation is called hard-core HRT (HC-HRT). The same kind of closure was used in [22] for a model of Kr involving both two-body and three-body interactions. Here, we adopt a new closure inspired by the SMSA integral equation which can be written as a local relationship between the direct correlation function $c(r)$ and the distribution function $h(r) = g(r) - 1$ [5]:

$$\begin{aligned} c(r) &= \phi(r) + g(r)\{1 - \exp[\beta v_R(r)]\} \\ &= c_R(r) + \phi(r) + [h(r) - h_R(r)]\{1 - \exp[\beta v_R(r)]\} \end{aligned} \tag{22}$$

where $v_R(r)$ is the (two-body) potential of the reference system and in the second line use has been made of the analogous equation satisfied by the direct correlation function of the reference system. SMSA has been shown to accurately reproduce the short-range correlations in simple fluids. The formal structure of this integral equation suggests that a realistic description of the short-range corrections to the mean-field approximation is given by the last term in (22). This information will now be used in the framework of HRT.

The parametrization of $\mathcal{C}_Q(r)$ is formally identical to the one already used for hard-core particles (19). The parameter λ_Q is again determined by the compressibility sum rule (20) which explicitly gives

$$\begin{aligned} \tilde{\mathcal{C}}_Q(k) = \tilde{c}_R(k) + \tilde{\phi}(k) + \frac{\tilde{\phi}(k)}{\tilde{\phi}(0)}\left[\frac{\partial^2}{\partial\rho^2}\left(\frac{-\beta\mathcal{A}_Q}{V}\right) - \tilde{c}_R(0) - \tilde{\phi}(0)\right] \\ + \left[\tilde{\mathcal{G}}_Q(k) - \tilde{\mathcal{G}}_Q(0)\frac{\tilde{\phi}(k)}{\tilde{\phi}(0)}\right]. \end{aligned} \tag{23}$$

This formula shows that the modified direct correlation function is given by the mean-field contribution plus two terms: the first takes care of the compressibility sum rule and is related to the density derivative of the free energy, while the second describes the short-range correlations induced by the attractive interactions. Here, however, the function $\mathcal{G}_Q(r)$

is not determined by the condition (21) which is only appropriate for hard-core molecules. Rather, $\mathcal{G}_Q(r)$ is now expanded in terms of a basis of short-range functions $u_n(r)$:

$$\mathcal{G}_Q(r) = \sum_{n\geqslant 1} \gamma_n^Q u_n(r) \tag{24}$$

where the coefficients γ_n^Q are determined by imposing the condition that the last term in equation (23) reproduces the short-range correlations in the same spirit as the SMSA integral equation (22). More precisely we first equate the last term of equation (23) to the last term of equation (22), evaluated for the partially interacting system:

$$\mathcal{G}_Q(r) - \tilde{\mathcal{G}}_Q(0)\frac{\phi(r)}{\tilde{\phi}(0)} = [h_Q(r) - h_R(r)]\{1 - \exp[\beta v_R(r)]\} \tag{25}$$

where the function $\mathcal{G}_Q(r)$ is parametrized via equation (24). Then we project equation (25) onto the basis $u_l(r)$, obtaining a set of coupled algebraic equations for the coefficients γ_n^Q:

$$\sum_{n\geqslant 1} \gamma_n^Q \int \mathrm{d}^3 r \ \exp[-\beta v_R(r)] u_l(r) \bar{u}_n(r)$$
$$= \int \mathrm{d}^3 r \ u_l(r)[h_Q(r) - h_R(r)]\{\exp[-\beta v_R(r)] - 1\} \tag{26}$$

where

$$\bar{u}_n(r) = u_n(r) - \frac{\tilde{u}_n(0)}{\tilde{\phi}(0)}\phi(r). \tag{27}$$

In our calculations we have chosen the basis functions as

$$u_n(r) = r^{n-1}\{1 - \exp[-\beta v_R(r)]\} \tag{28}$$

which is usually truncated after the first five terms, i.e. those with $n = 1, \ldots, 5$. Notice that equation (26) reduces, in the case of a hard-sphere reference system, to the usual core condition (21).

Equation (26) can be conveniently written in differential form, leading to evolution equations for the coefficients γ_n^Q as a function of Q. If we take the Q-derivative of equation (26) we obtain terms involving the derivative of γ_n^Q, which is the quantity of interest, and the derivative of $h_Q(r) = g_Q(r) - 1$. The evaluation of this Q-derivative should be performed with care because for a finite, non-zero, value of Q, $\tilde{h}_Q(k)$ is a discontinuous function of Q, related to $\tilde{\mathcal{C}}_Q(k)$ by the chain of equations

$$\rho^2 \tilde{h}_Q(k) = \tilde{F}_Q(k) - \rho \tag{29}$$

$$\tilde{F}_Q(k) = \begin{cases} \tilde{\mathcal{F}}_Q(k) & \text{if } k > Q \\ \tilde{\mathcal{F}}_Q(k)/[1 + \tilde{\mathcal{F}}_Q(k)\tilde{\phi}(k)] & \text{if } k < Q \end{cases} \tag{30}$$

$$\tilde{\mathcal{F}}_Q(k) = -\frac{1}{\tilde{\mathcal{C}}_Q(k)}. \tag{31}$$

Using these definitions we obtain

$$\sum_{n\geqslant 1} \frac{\mathrm{d}\gamma_n^Q}{\mathrm{d}Q}\rho^2 \int \mathrm{d}^3 r \ u_l(r) u_n(r) \exp[-\beta v_R(r)]$$
$$= \frac{Q^2}{2\pi^2}\tilde{P}_l(Q)\frac{[\tilde{\mathcal{F}}_Q(Q)]^2\tilde{\phi}(Q)}{1 + \tilde{\mathcal{F}}_Q(Q)\tilde{\phi}(Q)} - \int \frac{\mathrm{d}^3 k}{(2\pi)^3} \ \tilde{P}_l(k)[\tilde{F}_Q(k)]^2 \frac{\mathrm{d}\tilde{\mathcal{C}}_Q(k)}{\mathrm{d}Q} \tag{32}$$

where the function $P_l(r)$ is defined as

$$P_l(r) = u_l(r)\{1 - \exp[-\beta v_R(r)]\}. \tag{33}$$

The Q-derivative of $\tilde{\mathcal{C}}_Q(k)$ can be evaluated from equation (19); this gives

$$\frac{\mathrm{d}\tilde{\mathcal{C}}_Q(k)}{\mathrm{d}Q} = \frac{\mathrm{d}\lambda_Q}{\mathrm{d}Q}\tilde{\phi}(k) + \sum_{n\geqslant 1}\frac{\mathrm{d}\gamma_n^Q}{\mathrm{d}Q}\tilde{u}_n(k). \tag{34}$$

The derivative of the parameter λ_Q gives rise, via the compressibility sum rule (20), to two contributions:

$$\frac{\mathrm{d}\lambda_Q}{\mathrm{d}Q} = \frac{\mathrm{d}}{\mathrm{d}Q}\frac{\partial^2}{\partial\rho^2}\left(\frac{-\beta\mathcal{A}_Q}{V}\right)\frac{1}{\tilde{\phi}(0)} - \sum_{n\geqslant 1}\frac{\mathrm{d}\gamma_n^Q}{\mathrm{d}Q}\frac{\tilde{u}_n(0)}{\tilde{\phi}(0)}. \tag{35}$$

The first term is related to the building up of critical fluctuations as Q changes, being related to the Q-derivative of a quantity which in the limit $Q \to 0$ is proportional to the inverse of the compressibility. If the long-range fluctuations have little influence on the short-range behaviour of the system, the first term in (35) can be neglected, leading to

$$\frac{\mathrm{d}\tilde{\mathcal{C}}_Q(k)}{\mathrm{d}Q} \sim \sum_{n\geqslant 1}\frac{\mathrm{d}\gamma_n^Q}{\mathrm{d}Q}\bar{u}_n^Q(k). \tag{36}$$

When substituted into equation (32), the evolution equations for the coefficients γ_n^Q become

$$\sum_{n\geqslant 1}\frac{\mathrm{d}\gamma_n^Q}{\mathrm{d}Q}\left\{\rho^2\int \mathrm{d}^3r\; u_l(r)\bar{u}_n(r)\exp[-\beta v_R(r)] + \int\frac{\mathrm{d}^3k}{(2\pi)^3}\;\tilde{P}_l(k)[\tilde{F}_Q(k)]^2\bar{u}_n(k)\right\}$$
$$= \frac{Q^2}{2\pi^2}\tilde{P}_l(Q)\frac{[\tilde{\mathcal{F}}_Q(Q)]^2\tilde{\phi}(Q)}{1+\tilde{\mathcal{F}}_Q(Q)\tilde{\phi}(Q)}. \tag{37}$$

This set of equations must be supplemented by the initial condition

$$\lim_{Q\to\infty}\gamma_n^Q = 0 \tag{38}$$

expressing the obvious fact that the reference system satisfies the short-range condition imposed by the SMSA. Note that the approximation which decouples the long-range behaviour of the system from the core condition is the same as that used before in the context of the closure given by equation (19). Summarizing, the final numerical problem consists in the solution of the set of equations (16), (19), (20), (24), (37), and (38) together with the initial condition

$$\lim_{Q\to\infty}\left(\frac{-\beta\mathcal{A}_Q}{V}\right) = \left(\frac{-\beta A_R}{V}\right) - \frac{1}{2}\rho\phi(0) + \frac{\rho^2}{2}\tilde{\phi}(0). \tag{39}$$

We also have two boundary conditions, the first at low density given by the virial expansion of the equations, and the second at high density. This latter boundary condition has to be imposed at $\rho = \rho_{max}$, of the order of the density of the triple point and somewhat arbitrarily chosen. We have analysed the simple choice $\gamma_n^Q = 0$ and $\lambda_Q = 1$ at ρ_{max}. However, we have checked that the specific form of the boundary condition hardly affects the solution a few mesh points away from the boundary. Some detail on the numerical solution of this set of equations can be found in reference [24]. This approximation will be referred to as soft-core HRT (SC-HRT).

The closure (19), (23) amends some defects of the previously studied approximation to the HRT. In particular, it copes more naturally with soft-core potentials, which cannot be well represented by a hard-sphere reference system. However, it shares with the previous

closure a key approximation—that is, the fact that the regular (mostly attractive) part of the potential has been taken into account only linearly in the parametrization (19) of the direct correlation function. It is known [23] that this is satisfactory at densities of the order of that of the triple point, while it appears to be less accurate at intermediate densities and low temperatures.

It is clear that in this approximation (19), (24) the direct correlation function of the Q-system is an analytic function of k^2, so the critical behaviour of the system, in this approximation, belongs to the same class of Ornstein–Zernike closures as was previously analysed [4]. For example the divergence of the isothermal compressibility on the critical isochore is governed by the critical exponent $\gamma = 1.378$, while the Ornstein–Zernike exponent η vanishes. This should be compared with the experimental values $\gamma = 1.24$, $\eta = 0.025$.

4. The interaction model

The potential used here is the same as that in reference [22], namely the Aziz potential [25] for the two-body part with the parameters for krypton plus a three-body contribution of the Axilrod–Teller [26] form (Aziz + AT)

$$V(\boldsymbol{r}_1, \boldsymbol{r}_2, \ldots, \boldsymbol{r}_N) = \sum_{i<j}^{N} v_{\mathrm{Aziz}}(|\boldsymbol{r}_i - \boldsymbol{r}_j|) + \sum_{i<j<k}^{N} v_{\mathrm{AT}}(\boldsymbol{r}_i, \boldsymbol{r}_j, \boldsymbol{r}_k) \tag{40}$$

$$v_{\mathrm{AT}}(\boldsymbol{r}_1, \boldsymbol{r}_2, \boldsymbol{r}_3) = \frac{\nu(1 + 3\cos\Phi_1 \cos\Phi_2 \cos\Phi_3)}{r_{12}^3 r_{23}^3 r_{13}^3} \tag{41}$$

where the Φ_i are the angles of the triangles formed by the vectors $\boldsymbol{r}_i$ and $r_{ij} = |\boldsymbol{r}_i - \boldsymbol{r}_j|$, $i = 1, 2, 3$.

The division of the two-body potential into the attractive and repulsive parts is accomplished by defining

$$v_R(r) = \begin{cases} v_{\mathrm{Aziz}}(r) + \epsilon & \text{if } r < \sigma \\ 0 & \text{if } r \geqslant \sigma \end{cases} \tag{42}$$

$$w(r) = \begin{cases} -\epsilon & \text{if } r < \sigma \\ v_{\mathrm{Aziz}}(r) & \text{if } r \geqslant \sigma \end{cases} \tag{43}$$

where ϵ and σ are the depth of the attractive well and the position of the minimum. Note that the division adopted here is somewhat arbitrary even if it has been used frequently and with success in the literature [23].

In the HRT equation the reference system enters through the free energy and the structure factor. These quantities have been calculated using the MHNC equation with the potential given by equation (10) according to the procedure described in [1]. This implies that the effects of the Axilrod–Teller interaction on the reference system are calculated according to a scheme which is known to be fairly accurate in this respect. Each quantity was computed on a regular grid in the density–temperature plane and later interpolated for the required thermodynamic state. We checked that the results obtained did not depend upon the choice of the grid. Our calculations refer to a typical mesh of 500 points.

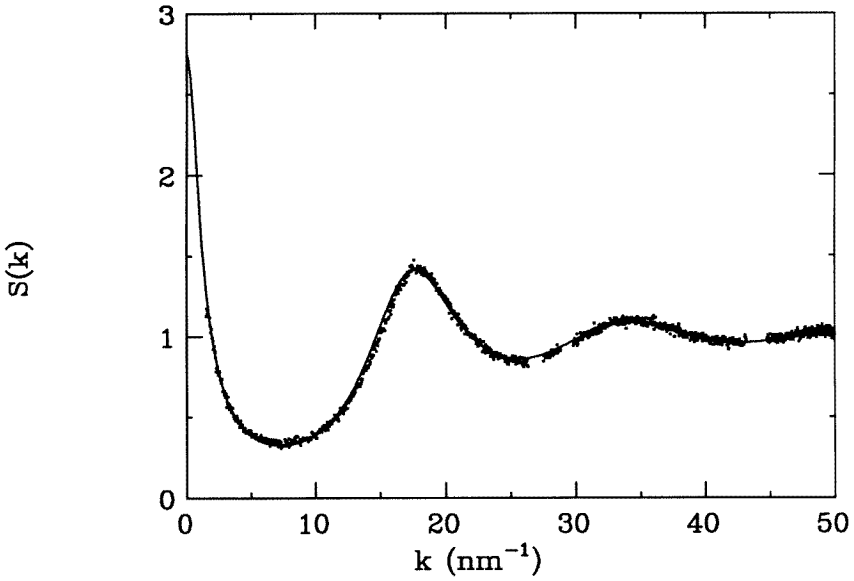

Figure 4. The structure factor for the state corresponding to experiment No 7 (points). Full line: SC-HRT results at the same reduced temperature.

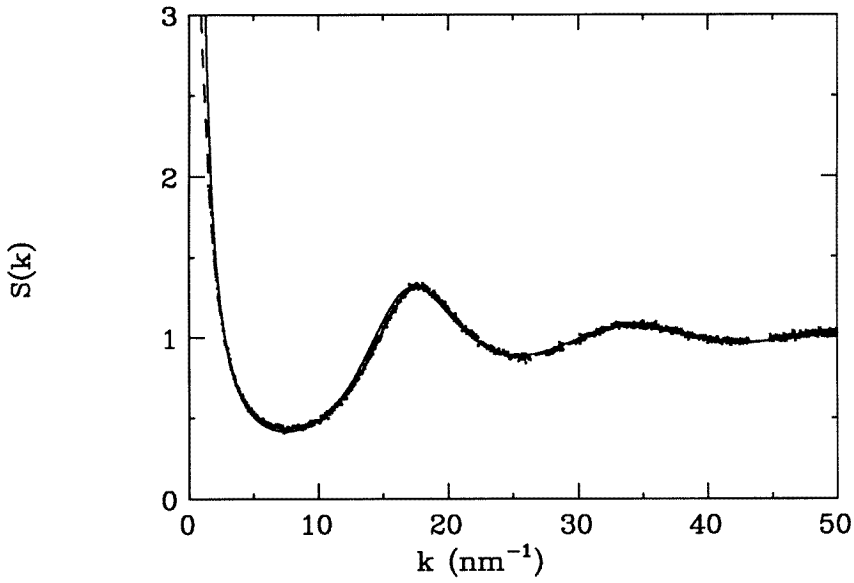

Figure 5. The structure factor for the state corresponding to experiment No 2 (points). Full line: SC-HRT results at the same absolute temperature. Dashed line: MHNC results.

5. Results

The experimental critical point of krypton is located at $\rho = \rho_c = 6.525$ atoms nm^{-3} and $T = T_c = 209.29$ K while the value for the compressibility factor $Z = P/\rho k_B T$ at

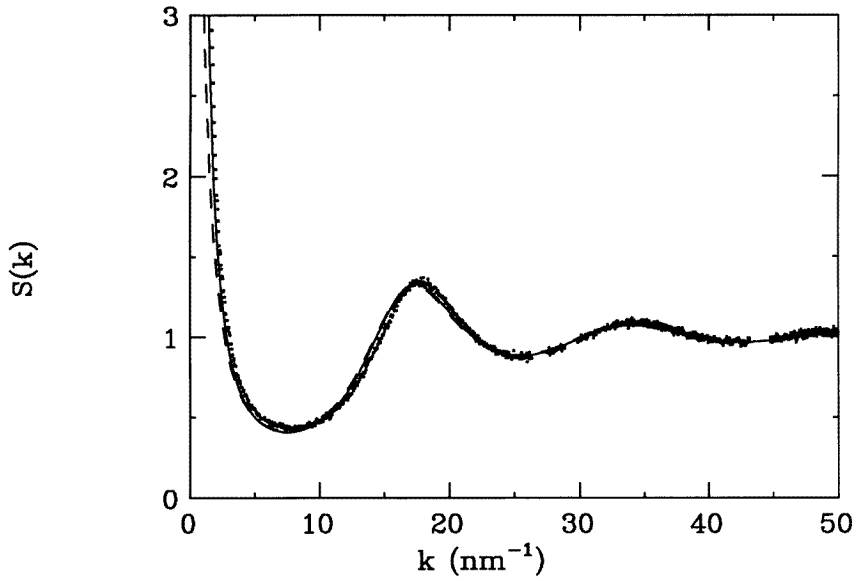

Figure 6. As figure 4, but for experiment No 5. The HC-HRT results are also shown (dashed line).

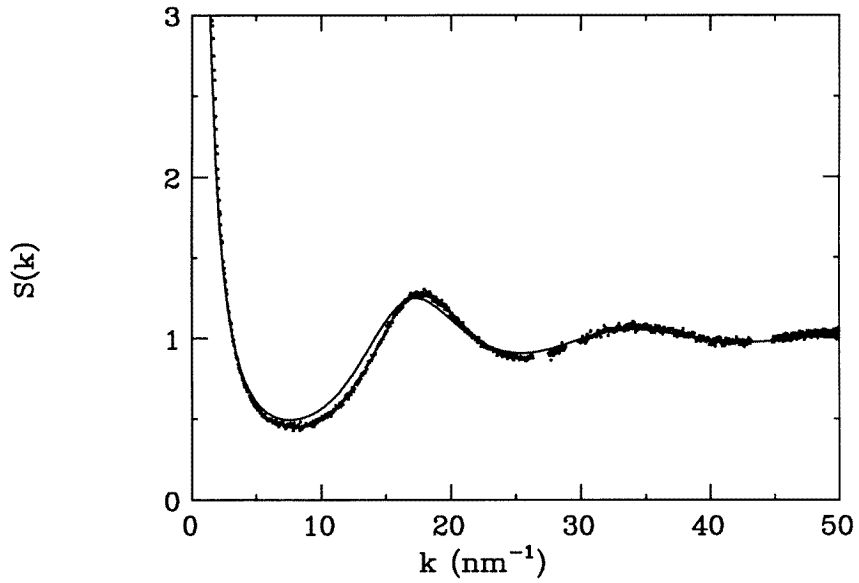

Figure 7. As figure 4, but for experiment No 8.

the critical point is $Z_c = 0.297$ [27]. Within SC-HRT, the critical point of the potential described above can be located, looking at the divergence of the isothermal compressibility at $\rho_c = 6.74$ atoms nm^{-3} and $T_c = 219$ K, i.e. the present theory gives a critical temperature higher than the experimental one, while for the critical density the agreement is acceptable.

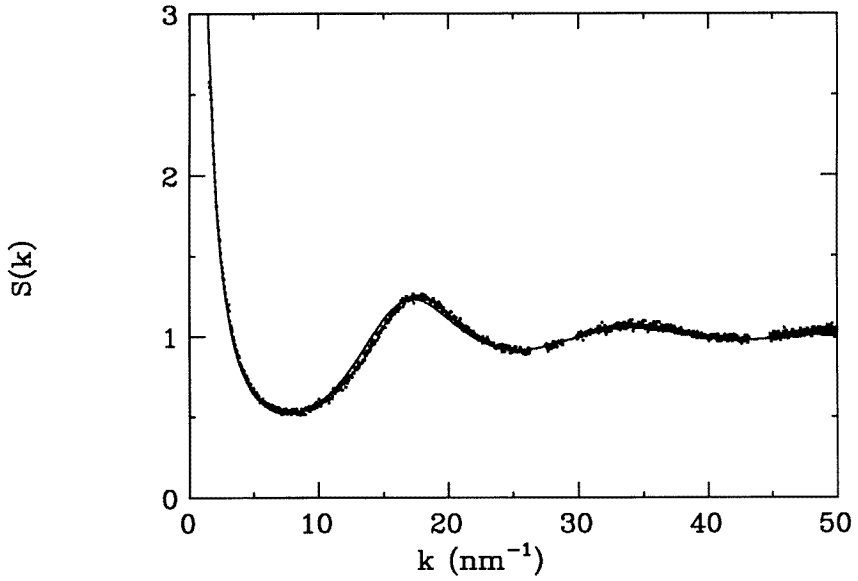

Figure 8. The structure factor for the state corresponding to experiment No 1 (points). Full line: SC-HRT results at the same absolute temperature.

The value of the compressibility factor is $Z_c = 0.31$. The same potential in the HC-HRT closure gave $\rho_c = 6.710$, $T_c = 220$ K and $Z_c = 0.307$ [22]. Finally the HC-HRT approach with only a two-body potential of the Aziz type gives a critical point at $T_c = 233$ K, $\rho_c = 7.082$ atoms nm^{-3} with $Z_c = 0.320$. This overestimation of the critical temperature by SC-HRT has at least two kinds of effect on the comparison of the theory with the experiment. First of all, some experimental points fall inside the theoretical coexistence curve; this is true particularly for the points which are nearest to the critical singularity. Secondly the $k \rightarrow 0$ limit of $S(k)$, being singular at the critical point, is very sensitive to small variations in the determination of the critical temperature. Therefore, the 5% difference in T_c between theory and experiment is crucial, especially for the comparison of the behaviour of $S(k)$ at small k. We contrast theory and experiment at the same reduced temperature, $(T - T_c)/T_c$, and the same density when possible. We have also made the comparison at the same absolute temperature in order to determine the effect of the change in temperature on short range correlations. We deal first with the short-range behaviour, looking at the region of k-values of the order of 5–50 nm^{-1}. Some examples of this comparison are presented in figures 4–8.

We discuss the data starting from the experiment at the highest density: in figure 4 $S(k)$ for experiment No 7 at the density 9.35 nm^{-3} is compared with SC-HRT at the same reduced temperature. One can see that there is an overall very good agreement at all k. There is only a hint of a displacement of the main peak of $S(k)$ to a smaller k-value. When the computation is performed at the same T as for the experiment, the theoretical curve is almost unchanged. For the density 7.25 nm^{-3} we display the results for two temperatures. In figure 5 the $T = 227$ K data (experiment No 2) are shown and in figure 6 the $T = 210$ K case (experiment No 5), the temperature closest to the critical isotherm in the present experiment. There is an overall good agreement, but now the displacement of the position of the main peak of the theoretical structure factor becomes more appreciable (about 2%)

and the peak height is slightly smaller than the experimental one. These deviations become rather pronounced for the experimental density 5.80 nm^{-3}: the results of experiment No 8 are shown in figure 7. Finally the data at density 5.38 nm^{-3} (experiment No 1) are shown in figure 8. Here the agreement between theory and experiment is again quite good. We can summarize by saying that for all of the states except the two at density $\sim$5.80 nm^{-3} (experiments No 8 and No 9) the agreement between theoretical and experimental results is within seven parts per hundred in the small- and intermediate-k regions up to 25 nm^{-1}, and is within two parts per hundred for higher k-values up to 50 nm^{-1}. The disagreement between HRT and the two experiments at density $\sim$5.80 nm^{-3} is puzzling, because for all of the neighbouring thermodynamic states at higher and lower density and temperature closer to and further from T_c, we find better agreement. It seems worth repeating the experiment for the 5.80 isochore.

We have performed computations also with the previous version of HRT, the HC-HRT in which hard spheres are used as a reference system. SC-HRT gives systematically better results than HC-HRT and, as an example, in figure 6 the HC-HRT data are also shown. The deviation between HC-HRT and experiments is about twice as large as that of SC-HRT for all of the thermodynamic states of the present experiment.

In the case of experiments 1 and 2, which are located rather symmetrically with respect to the critical density, at a reduced temperature $t = (T - T_c)/T_c$ of the order of 10^{-1} it was possible to make a detailed comparison between the experiments and the results of different theories and interaction models. First of all, the comparison between the MHNC and SC-HRT approximations and experiments at the same absolute temperature is favourable to MHNC for this range of k, the difference between MHNC and HRT being of the same order as the discrepancy between the MHNC results and the experiment. The effect of the three-body potential on the structure in SC-HRT is small for these temperatures, and in the direction of systematically improving the agreement with the experiments. The comparison was for obvious reasons made at the same reduced temperature. The three-body potential has a large effect, mainly on the equation of state, which gives rise to a sizable change in the small-k range of $S(k)$ if the comparison is made at the same absolute temperature.

The comparison in the range of k of the order of 1.5–5 nm^{-1} is presented in figures 9 and 10. The usual way to analyse the data is in terms of an Ornstein–Zernike (OZ) plot of $1/S(k)$ versus k^2. The Ornstein–Zernike theory [23] predicts that for sufficiently small k the behaviour should be given by the law

$$\frac{1}{S(k)} = \frac{1 + \xi^2 k^2}{S(0)}.$$

For sufficiently small values of k and sufficiently near the critical point, deviations from the OZ behaviour are expected due to the non-vanishing value of the critical exponent η. However, the smallness of η ($\sim$0.03) hides this effect, at least for the range of k and for the thermodynamic states that we investigated in these experiments. In all cases the experimental data follow this law at sufficiently small k. The largest discrepancy between the experiments and SC-HRT is within 5%, the difference being smaller in the vast majority of the cases. The experimental data seem more rectilinear than the SC-HRT results, an indication that the effects of higher-order terms in k are overestimated by HRT. Firm conclusions on this point have to wait for measurements at smaller k.

With the same data it is possible to compute several interesting properties, for example the density derivative of $\tilde{c}(k)$ and that of $\tilde{h}(k)$. These quantities are valuable because they are related to three-body correlations, giving other important information about the structure of the system. We present the density derivative for three thermodynamic states

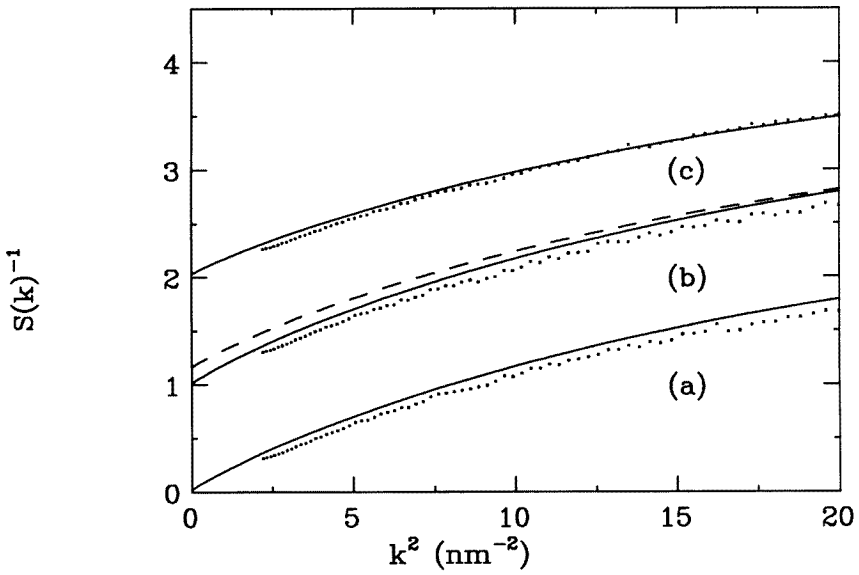

Figure 9. OZ plots for experiments No 4 (a), No 5 (b), and No 9 (c) (points) compared with SC-HRT at the same absolute temperature (full lines). For experiment No 5 the HC-HRT results are also shown (dashed line). Data (b) and (c) have been shifted upwards for clarity.

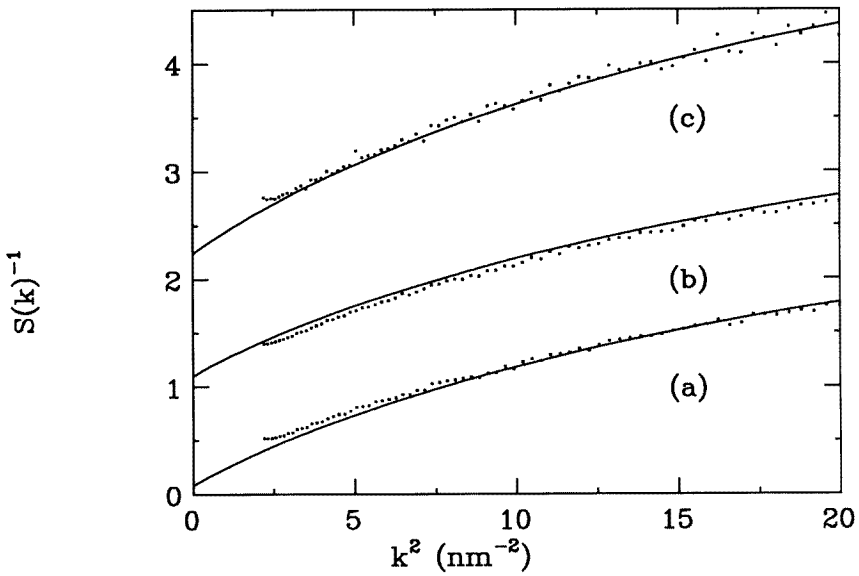

Figure 10. OZ plots for experiments No 2 (a), No 3 (b), and No 6 (c) (points) compared with SC-HRT at the same reduced temperature (full lines). Data (b) and (c) have been shifted upwards for clarity.

using respectively the data from experiments 1 and 2, 3 and 7, and 4 and 6. The theoretical results for the derivatives have been obtained by use of the same finite increments as in

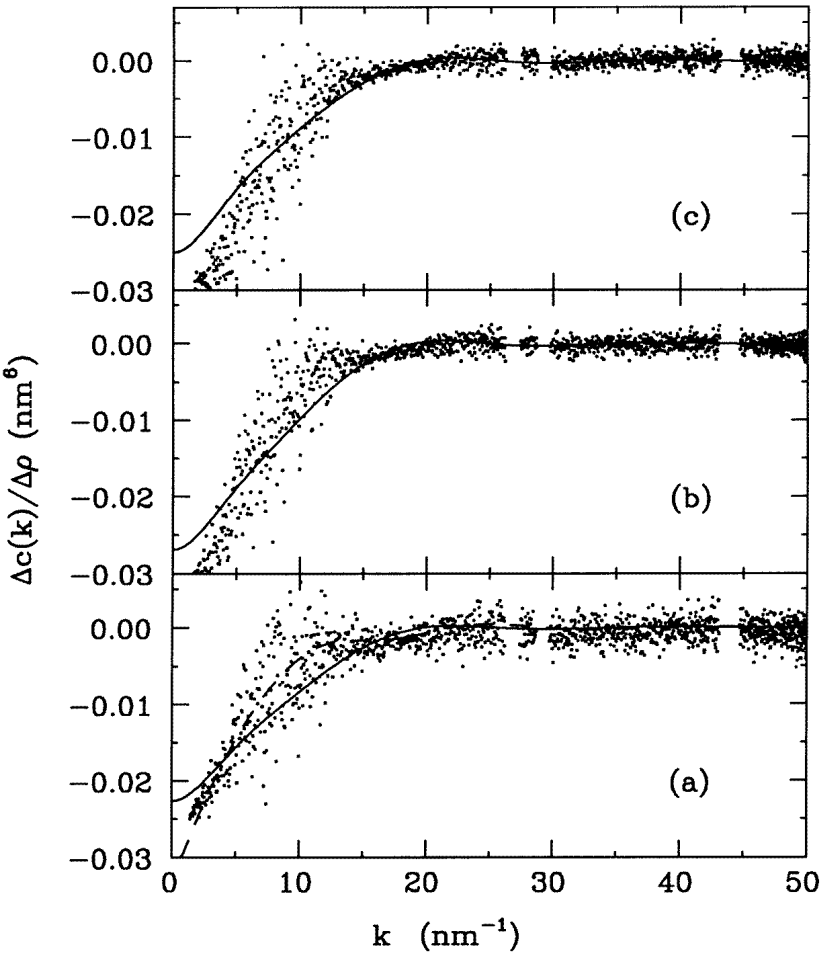

Figure 11. Density derivatives of the direct correlation function from experimental data: from experiments Nos 1 and 2 (a), 3 and 7 (b), and 4 and 6 (c). Points: experiments. Full line: SC-HRT. Dashed line: MHNC data.

the experiments. By considering smaller density increments we have verified that what we present are *bona fide* representations of the actual derivatives. The experimental data give results which are rather noisy, so we can only discriminate the main features of the theory. In all of the three cases the only structure which can be clearly identified in $\partial\tilde{c}(k)/\partial\rho$ (see figure 11) is a smooth behaviour starting from a value of the order of -0.03 nm^6 at small k and rising to zero for $k \sim 15$ nm^{-1}. The same feature is present in SC-HRT, but the theory seems to predict a less negative value at small k. Instead, for $k \geqslant 20$ nm^{-1} the function $\partial\tilde{c}(k)/\partial\rho$ predicted by SC-HRT is very small, in agreement with experiments. The same behaviour is also given by the MHNC approach.

The results for $\partial\tilde{h}(k)/\partial\rho$ are given in figure 12. This quantity has a more pronounced structure than $\partial\tilde{c}(k)/\partial\rho$. The experimental data give a well defined maximum at $k \sim 7$–8 nm^{-1} and a minimum at $k \sim 15$–17 nm^{-1}. These features are well represented by SC-HRT in all three cases. The theory gives also a weak maximum at $k \sim 18$–19 nm^{-1} but this is

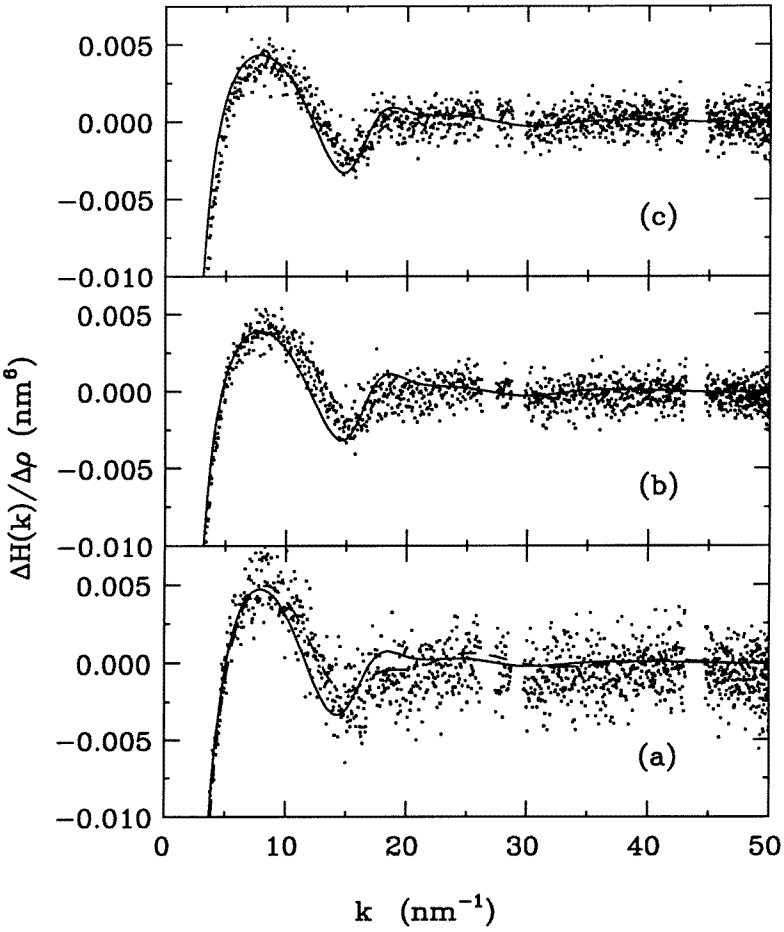

Figure 12. As figure 11, but for the density derivative of $\tilde{h}(k)$.

too shallow to be seen in the present experiment. At higher densities this weak maximum becomes a well developed structure, and this was seen experimentally [1].

6. Conclusions

We have shown that advances in the experimental techniques and in the theory make feasible a complete comparative study of static correlations in the critical region over all of the significant length scales. On the theoretical side, it is known that HRT is a scheme which embodies the merits of integral equations in the description of correlations at short distance with those of the renormalization group for the treatment of long-range correlations. By coping directly with the soft-core part of the interaction we now have a theory (SC-HRT) which provides realistic functions $g(r)$ and $S(k)$ for accurate models of two- and three-body potentials. In this theory, both functions develop the proper scaling behaviour at large distance when the critical point is approached. It is unique to SC-HRT to have all of these features. When the thermodynamic state is not too close to the critical point, and hence an

accurate integral equation like the MHNC one has a solution, comparison of SC-HRT and MHNC results with experiments indicates that the MHNC approach is slightly superior to SC-HRT in the description of correlations at short distance. On the other hand, HRT can approach arbitrarily close to the critical point.

The critical temperature given by SC-HRT is about 5% higher than the experimental one. This deviation is larger than in the case of the LJ system where HRT overestimates T_c by 2%. Such a discrepancy can have different origins.

(i) The Aziz potential has a deeper attractive well compared to the LJ one, so the closure (23) adopted might be less accurate.

(ii) The three-body AT potential gives rise to an effective, repulsive, two-body contribution which has the same r^{-6}-behaviour at large distance as the pair interaction, thereby reducing the strength of the attractive tail. Therefore, the inclusion of the full AT potential in the reference system could be not fully justified and a treatment of the effective two-body AT interaction on the same grounds as the attractive tail seems more appropriate.

(iii) The model potential which we have used does not represent the true interatomic interaction of Kr.

We believe that item (ii) is indeed significant and that the present scheme underestimates somewhat the depression of T_c due to the AT interaction. It should be possible to improve the theory in this respect. It is important to reduce the deviation in T_c at the level of 1–2% because in this case the use of the same reduced temperature as in the experiments will leave the short-range part of the correlations essentially unaltered.

From the experimental point of view, the present measurements touch the critical regime of fluctuations only superficially, because the k-range does not extend to small enough values to probe the scaling behaviour in depth. High-precision measurements at smaller k are possible, and the present results suggest that such an experiment should be performed. This will allow a fruitful comparison between theory and experiment, giving information on a number of questions like those of the extension of the scaling regime for the structure factor, the form of the corrections to scaling, and the influence of the long-range parts of the pair and triplet interactions, which give rise to k^3-contributions to $S(k)$, in the critical region [28]. In the case of a fluid, not much is known on these questions, which concern the non-universal part of the critical behaviour.

Acknowledgments

The valuable technical assistance of M Neri of Dipartimento di Fisica, Universita' di Firenze, and of the Cryogenics Group of the Institut Laue–Langevin was essential to the accomplishment of the experimental part of the present study.

References

[1] Barocchi F, Chieux P, Magli R, Reatto L and Tau M 1993 *Phys. Rev. Lett.* **70** 947
Barocchi F, Chieux P, Magli R, Reatto L and Tau M 1993 *J. Phys.: Condens. Matter* **5** 4299
[2] Rosenfeld Y and Ashcroft N W 1979 *Phys. Rev.* A **20** 1208
[3] Poll P D and Ashcroft N W 1985 *Phys. Rev.* A **32** 1722
[4] Parola A and Reatto L 1995 *Adv. Phys.* **44** 211
[5] Zerah G and Hansen J-P 1986 *J. Chem. Phys.* **84** 2336
[6] Streett W B and Staveley L A K 1971 *J. Chem. Phys.* **55** 2495
[7] Egelstaff P A 1987 *Methods of Experimental Physics* vol 23, part B, ed D L Price and K Sköld (New York: Academic)

[8] van Laar B and Yelon W B 1984 *J. Appl. Crystallogr.* **17** 47 and references therein
[9] Fredrikze H 1988 Private communication
[10] Fredrikze H, van Tricht J B, van Well A A, Magli R, Chieux P and Barocchi F 1989 *Phys. Rev. Lett.* **62** 2612
[11] Soper A K, Howells W S and Hannon A C 1989 *Rutherford Appleton Laboratory Report* RAL-89-046
[12] Chieux P 1992 Private communication
[13] Paalman H H and Pings C J 1962 *J. Chem. Phys.* **33** 2635
[14] Yarnell J L, Katz M J, Wenzel R G and Koenig S H 1973 *Phys. Rev.* A **7** 2130
[15] Placzek G 1952 *Phys. Rev.* **86** 377
[16] Fredrikze H 1988 *Phys. Rev.* A **36** 2272
[17] Verlet L 1968 *Phys. Rev.* **165** 201
[18] Teitsma A and Egelstaff P A 1980 *Phys. Rev.* A **21** 367
[19] Youden J A 1987 *MSc Thesis* University of Guelph, Ontario
[20] Parola A and Reatto L 1985 *Phys. Rev.* A **31** 3309
[21] Meroni A, Parola A and Reatto L 1990 *Phys. Rev.* A **42** 6104
[22] Meroni A, Reatto L and Tau M 1993 *Mol. Phys.* **80** 997
[23] Hansen J-P and McDonald I R 1986 *Theory of Simple Liquids* 2nd (New York: Academic)
[24] Tau M, Parola A, Pini D and Reatto L 1995 *Phys. Rev.* E **52** 2644
[25] Aziz R and Slaman M 1986 *Mol. Phys.* **58** 679
[26] Axilrod B M and Teller E 1943 *J. Chem. Phys.* **11** 299
[27] Sengers J V and Levelt J M H Sengers 1986 *Annu. Rev. Phys. Chem.* **37** 189
[28] Reatto L and Tau M 1987 *J. Chem. Phys.* **86** 6474